Analysis of liquid spray structures using two-photon fluorescence laser sheet imaging

Hannah Ulrich[1,2], Bastian Lehnert[1,2], Diego Guénot[4], Kristoffer Svendsen[4], Olle Lundh[4], Stefan Will[1,2], Michael Wensing[1,2], Edouard Berrocal[2,3], Lars Zigan[1,2]

[1]Lehrstuhl für Technische Thermodynamik (LTT),
Friedrich-Alexander-Universität Erlangen-Nürnberg (FAU), Erlangen, Germany
[2]Erlangen Graduate School in Advanced Optical Technologies (SAOT),
Friedrich-Alexander-Universität Erlangen-Nürnberg (FAU), Erlangen, Germany
[3]Division of Combustion Physics, Lund University, Lund, Sweden
[4]Division of Atomic Physics, Lund University, Lund, Sweden
*Corresponding author email: hannah.ulrich@fau.de

Abstract
In this work two-photon laser-induced fluorescence (2p-LIF) laser sheet imaging is used to analyze the structure and the atomization behavior of water and ethanol sprays. Multiple light scattering is reduced by 2p-LIF measurements using a femtosecond laser. This allows high-contrast spray imaging close to the nozzle resulting in an improved identification of single liquid structures. A commercial 6-hole DISI (Direct-Injection Spark-Ignition) injector was studied at different injection pressures, operated with ethanol and water containing a LIF dye (fluorescein). Compared to water, the ethanol spray structure shows increased cone angles in the nozzle near-filed. For the size of the liquid structures, no clear dependency on the fluid properties is observed in this spray region.

Keywords
2p-LIF; fluorescence; liquid structures; atomization; cyclic variations

Introduction

Water and ethanol are both common solvents in various spraying processes such as painting, cooling, particle synthesizing and fuel combustion. Thus, the analyzation of such sprays is useful for a further understanding of atomization in manifold energy and process engineering applications.

In spray imaging there is a great variety of approaches to examine the characteristics of the liquid jets. The range of conventional methods extends from macroscopic and microscopic imaging over planar and 3D measurements to qualitative and quantitative analyzations. Each region of the spray has a different characterization and thus variable visualization techniques have emerged in the last decades [1]. As for the nozzle near-field, the sprays are usually very dense and hence the illumination and detection of the spray structure suffer from multiple light scattering. The majority of the detected photons have been scattered multiple times by ambient off-axis liquid structures. This effect leads to a masking of the investigated liquid structures in the core spray [2, 3, 1]. In recent years, various measurement techniques such as X-ray radiography, ballistic imaging (BI) or structured laser illumination planar imaging (SLIPI) have been established for the attempt to suppress multiple scattering [4, 2, 5].

One approach to circumvent the detection of multiply scattered photons is to suppress the light, which is scattered by structures from outside of the focus plane. For example, in BI the photons refracted by large fluid structures are preserved while multiply scattered photons are filtered to avoid misleading effects [6, 5]. Another way to correct corruption of the data is

filtering the erroneously detected photons in the post processing. This method is applied in SLIPI where a spatially modulated laser sheet is used to visualize the spray [7, 8].

In a previous work, Guénot et al. [3] introduced the combination of X-ray and 2p-LIF measurements to get insight into the detailed spray structure. Both techniques avoid the generation of multiple scattering and thus the intensity of the ambiguous off-axis signals is insignificant. The approach of 2p-LIF is based on the probability of a simultaneous absorption event of two photons. This probability is high in the focus plane, where the liquid structures absorb the fs-laser light and emit fluorescing photons. In the turbid spray region outside of the laser light sheet, the scattering effects occur with a wide spatial and temporal distribution. Consequently, the energy of an absorbed photon in the fluorescence dye is insufficient to elevate electrons from their electronic ground state to an excited state. This means that the dye will not show fluorescence in case of 1-photon excitation. 2p-LIF has been widely applied in e.g. biological microscopy [9] or in flame species measurements [10–12]. Berrocal et al. [2] introduced this technique to visualize atomizing water sprays and presented a comparison to the common single-photon LIF approach.

In this work, we continued the investigations by operating the injector with different liquids and fuels at different injection pressures with a detection at various times during the injection (after the visible start of injection (vSOI)). Consequently, the measurements allow for a detailed comparison of the fluid-dependent breakup process and the resulting liquid structures in dense sprays.

The influence of fluid properties on the spray structure is often discussed within the scope of internal nozzle flow investigations. Various groups analyzed the correlation of fuel dependent cavitation and turbulence of the nozzle flow on the spray shape and atomization [13–15]. It is known that both cavitation and turbulence increase with lower viscosity [13]. Consequently, with lower viscosity, the liquid velocity of the spray exiting the nozzle may be elevated accordingly and due to the flow not being decelerated at the nozzle wall, a reduced cone angle is expected [14].

The fluid properties like surface tension and viscosity determine the size, shape and local distribution of the resulting liquid structures, as well as the spray width and cone angle. The latter are also analyzed in this paper in terms of cyclic variability of the macroscopic spray shape, which determine the atomization quality, droplet dispersion as well as the subsequent mixing process.

Material and Methods

The measurements were performed using a titanium-sapphire chirped pulse amplification system at Lund High-Power Facility, further described in ref. [16]. The light intensity needs to be sufficient to overcome the energy gap of the fluorescent molecules with two photons. Therefore, the femtosecond laser generates pulses with a pulse energy of 10 mJ and a duration of 38 fs. With a center wavelength of 800 nm, two photons match the necessary energy for a 2-photon fluorescence of the LIF dye fluorescein. A fraction of 0.1 % fluorescein is added to both investigated liquids, water and ethanol. The equivalent fuel properties were determined to be unaffected by adding only this small amount of dye [3]. For the measurements a commercial 6-hole DISI injector with one definable spray cone is studied. The injector is operated at three different injection pressures of 10 MPa, 20 MPa and 30 MPa. Four different time steps after the visible start of injection are recorded.

The imaging system of the setup is depicted in Figure 1. A cylindrical lens with a focal length of 150 mm was utilized to generate a light sheet of ~2 cm x 100 µm at the nozzle exit. The

detection system consists of a telecentric lens combined with a high resolution 5.5 megapixel sCMOS camera (Andor Zyla 5.5) resulting in a 6.5 µm pixel resolution.

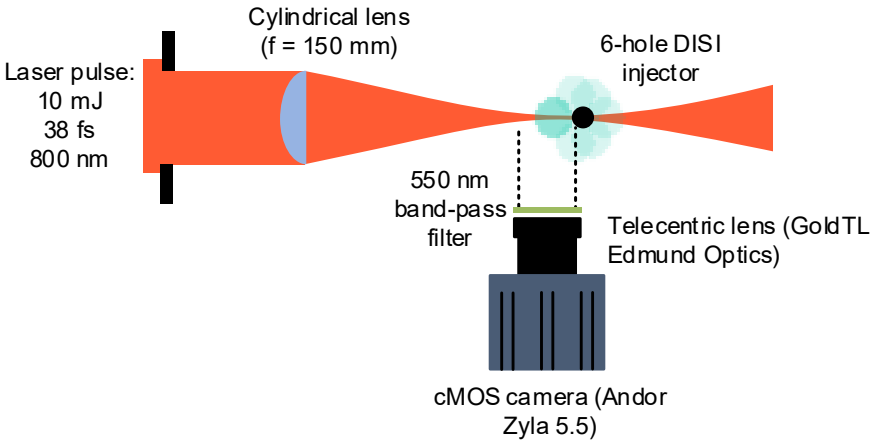

Figure 1. Optical setup for the 2p-LIF measurements.

For additional comparison, further images are taken with backlight illumination. For this purpose, the laser beam was directed straight to a fluorescing background behind the spray. Hence, the detection system collects a shadowgraphy image of the spray. These images are only used to reassess the information obtained by the 2p-LIF measurements.
The post-processing consists of a binarization of the maximal recorded 50 single-shot images. For this purpose, an intensity threshold of 25/255 is set for the converted 8-bit pictures. This value is chosen to separate between in-focus liquid structures ($\geq$ 25) and “background/ noise signal” (< 25), which consists of camera noise and possibly fluorescence signal of very small droplets in the plane of the laser sheet. For the determination of the near-field cone angle, a linear interpolation of the radial spray boundary is conducted from the nozzle exit up to a 1 mm distance from the nozzle. The angle of the spray is measured within this region for the single-shot images. A 95 % confidence interval is calculated using Student’s t-distribution.
Additional post-processing provides information about the dimensions of the liquid structures located in the area up to 4 mm distance from the nozzle exit. An analysis of all structures with an overall size > 15 pixel rejects droplets and small ligaments to reduce an overestimation of the size due to the resolution. All larger structures are evaluated by measuring Feret’s diameter (which is the maximum distance between any two points of the liquid body).

Results and Discussion

Figure 2 shows the liquid structures of a water and an ethanol spray. With the suppression of multiple light scattering, the main advantage of the 2-photon approach, it was possible to image the core of a single spray plume. Generally, the recorded images provide deep insights into the atomization behavior including the emerged formations of ligaments, clusters and droplets. However, in these 2p-LIF-images, the right part of the plume appears blurred. In these areas, the spray plume merges with the other jets. The fluorescence signal originates from small droplets emanating from the out of focus spray plumes. These small structures refract the light randomly and not in unison. The spatial and temporal dispersion of secondary scattered fluorescence photons could also lead to a LIF signal in these regions. An attenuation of the fluorescence signal can be related to reabsorption effects of the dense spray covering the jet under study.

For clarification, an exemplary shadowgraphy image is shown in Figure 3 in comparison to an inverted raw 2p-LIF intensity image. By including the shadowgraphy images, the position of the adjacent off-axis spray cones is estimated. In the region of the single spray plume, the fluorescence image shows a clear signal. As for the interference with the remaining spray jets, the intensity signal gets blurry and prevents a clear separation of the single plumes.

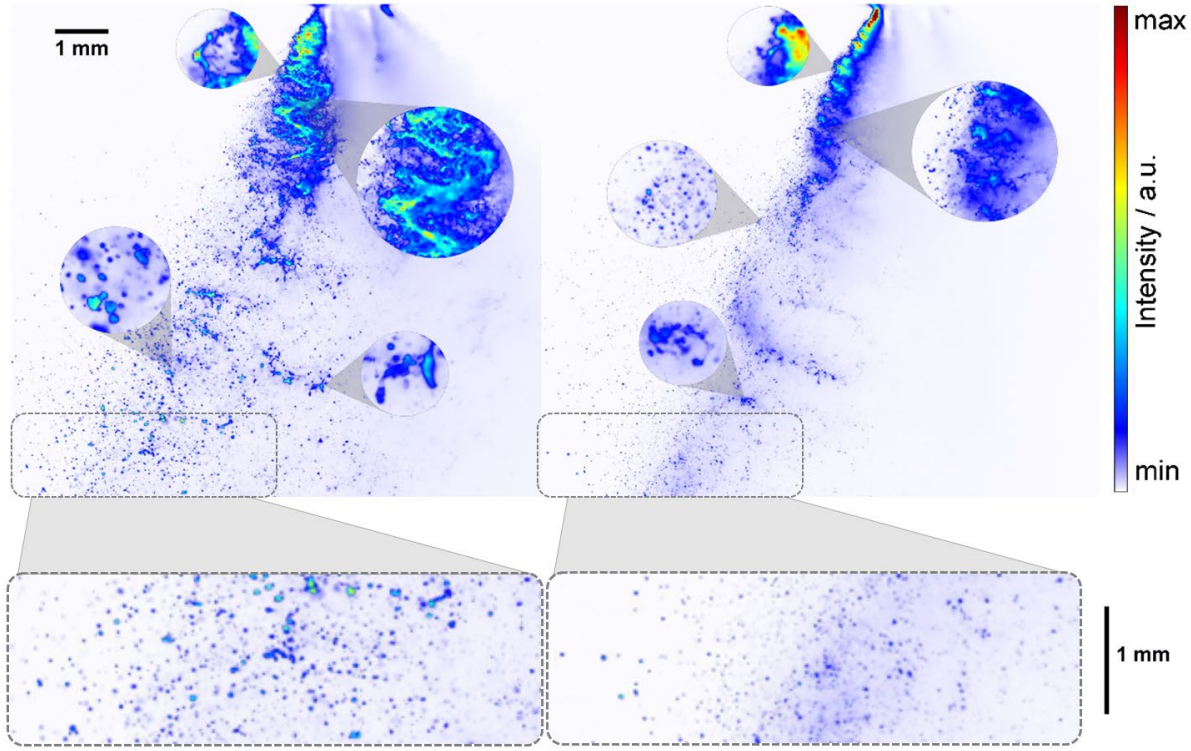

Figure 2. Liquid fuel structure of a single plume of a water (left) and an ethanol spray (right) including magnifications of ligaments, wavy jet breakup zones, clusters and droplets in the nozzle far-field.

Consequently, in the subsequent analysis, the spray cone angle is related to the left boundary of the spray and the injector axis (which is the vertical direction of the spray propagation). The width of the spray plume cannot be determined reliably.

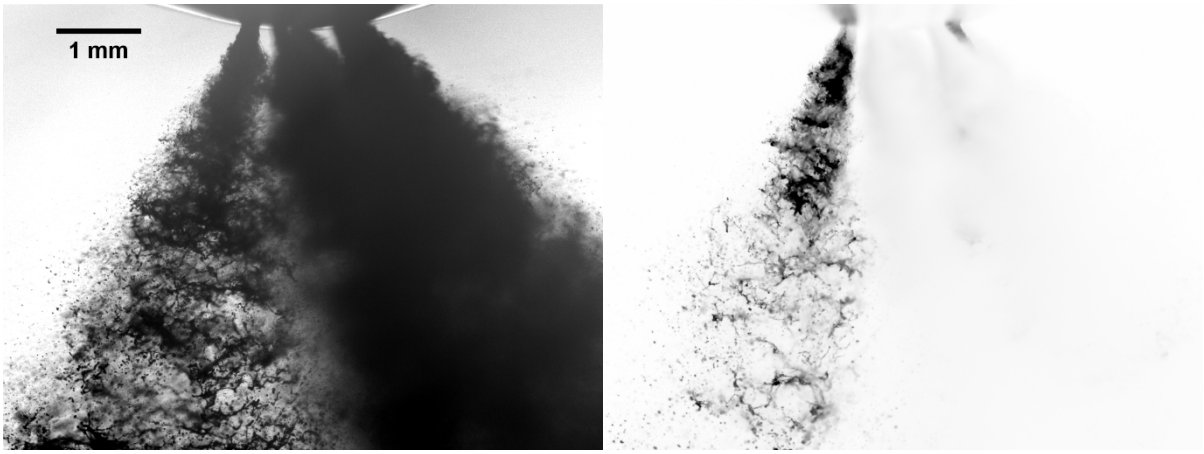

Figure 3. Shadowgraphy image (left) and an inverted 2p-LIF image (right) of the water spray at 20 MPa and 220 µs after vSOI.

In the next paragraph, the effect of the fluid properties on the spray shape and structure is analyzed. Two main properties determining the nozzle flow and atomization are the viscosity and the surface tension. The values and resulting Reynolds (Re) and Weber numbers for liquids (We_L) are shown in Table 1. Due to its high surface tension, a significantly smaller Weber number is obtained for water. The enlarged sections in Figure 2 show a difference in drop sizes in the nozzle far-field (i.e. at the spray front). Based on the lower Weber number a comparably slow breakup is expected for water, explaining the larger droplets [17].

Table 1 – Fluid properties and dimensionless numbers of ethanol and water at 293 K and 0.1 MPa [18, 19]

	density (kg/m^3)	dynamic viscosity (mPa·s)	surface tension (mN/m)	Re	We_L
ethanol	789.42	1.194	22.39	13,397	113,450
water	998.21	1.002	72.88	17,955	44,457

In addition, the Reynolds number is determined, which is more than 30 % larger for water than it is for ethanol. As for the fluid behavior, increased turbulence and cavitation inside the nozzle are expected for larger Reynolds numbers while a smaller cone angle is probable [14, 13].
The resulting spray cone angle is provided in Figure 4 for various injection pressures (left) and points in time (right). As anticipated, the resulting spray angles for water are smaller for all injection pressures and points in time studied.
The angle of the ethanol spray at 220 µs shows a steady incline with rising injection pressure. This is due to the increased velocity difference between spray and air with larger injection pressure. Consequently, the spray is pushed aside of its original propagation direction resulting in a broadened spray plume. The same trend was reported for the near-nozzle cone angle of DISI spray for a pressure change from 5 MPa to 10 MPa [20]. For water, a similar tendency is observed for the lower injection pressures. At 30 MPa injection pressure, the measurements reveal a lower angle for water than it was evaluated for 20 MPa. In general, the increased confidence intervals for both liquids at higher pressures indicate a rise of the cyclic variations, which can be explained by larger wrinkling of the liquid surface in the near-nozzle region.
Regarding the time-dependent behaviour, both liquids show a similar trend. The incipient nozzle near-field cone angle is small, while in the subsequent time step, a strong increase is observed, which can be explained by the increasing flow velocity during needle opening. When the needle is fully opened, the nozzle flow is in a more stationary phase leading to a further decline with advanced time and reduced standard deviations [20].

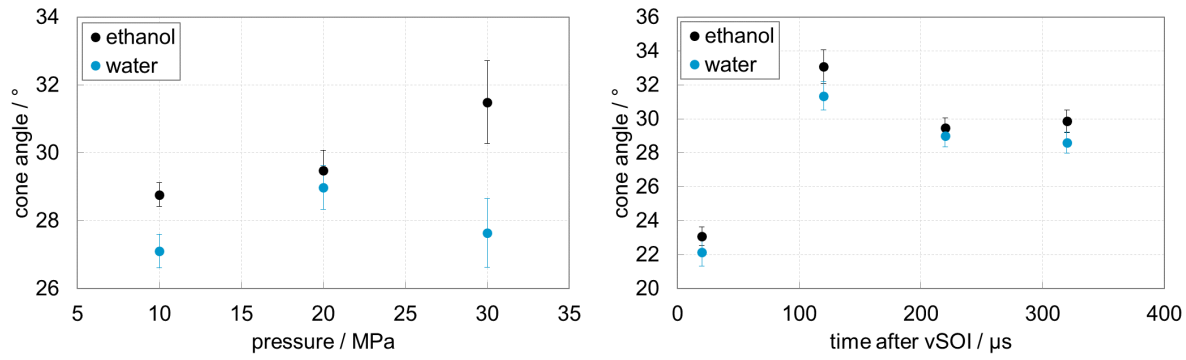

Figure 4. Injection pressure dependent cone angle at 220 µs (left) and time dependent cone angle at 20 MPa (right) with 95 % confidence interval.

Regarding Feret's diameter of the liquid structures in the near-nozzle region, no clear trend relating to the liquid properties could be observed. The pressure (left) and time-dependent (right) variation of the mean values including the 95 % confidence intervals are presented in Figure 5. The analysed liquid structures show average dimensions of about 80 µm-130 µm.
For water, the length of the liquid structures is reduced with an increase of the injection pressure. At high injection pressures, the flow is accelerated and the Reynolds number rises. The intensified turbulence and aerodynamic breakup results in smaller spray structures. Ethanol shows a different break-up behaviour with larger structures at 20 MPa. At 30 MPa the turbulent break-up predominates, which may be supported by cavitation-induced breakup, leading to smaller Feret's diameters.

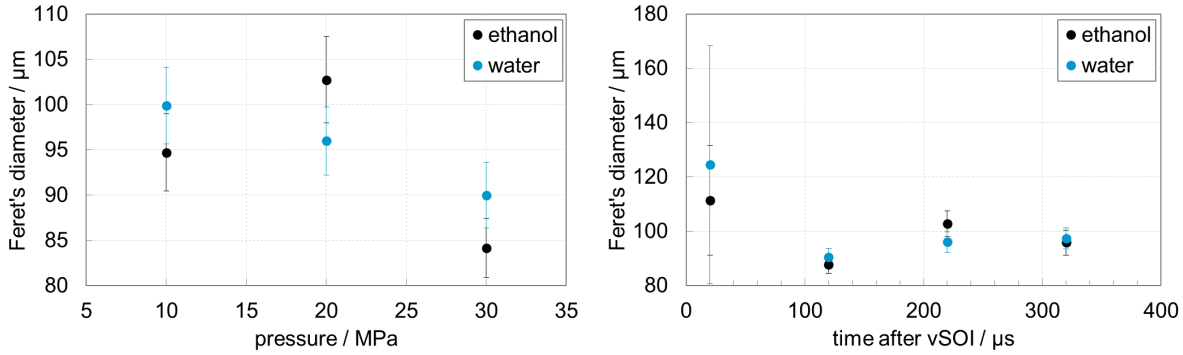

Figure 5. Injection pressure dependent Feret's diameter at 220 µs (left) and time dependent Feret's diameter at 20 MPa (right) with 95 % confidence interval.

At the incipient time step, high values for Feret's diameter with large fluctuations are observed. The images show only very little break-up of the spray, which explains the (few) larger liquid structures and the augmented confidence intervals. Due to further spray break-up, the subsequent decline in the diameter was presumed. For the following time steps, the spray front exceeds the analysed region, leading to a shift to slightly larger structures. In principle, the size of the liquid bodies is very similar for both liquids in the near-nozzle region. In ref. [20] the differences in structural dimensions depending on the liquid viscosity and surface tension were also small in general, although a higher number of large structures were observed for a fuel with (much) larger viscosity. Probably, a larger number of images is necessary for clearer dependencies of Feret's diameter on the liquid properties.

Conclusions

The 2p-LIF approach was applied to a common DISI injector to observe differences in the spray structures depending on the liquid properties. A high-resolution imaging of the dense spray core enabled a comprehensive analysis of the atomization process close to the nozzle exit. The recorded images were evaluated in terms of the cone angle and liquid structure lengths in the nozzle near-field. The basic presumption of higher viscosities resulting in increased plume angles could be verified. Lower Reynolds numbers lead to an enlargement of the spray angle. Higher injection pressures showed an increased spray broadening, larger cone angles and smaller liquid structures for both tested liquids. Largest cyclic variations were observed during needle opening, i.e. early points in time after start of injection. By taking further spray regions and time steps into account, better statistics could be achieved in future measurements.

Acknowledgements

The authors gratefully acknowledge the financial support for parts of this work by the European Union's Horizon 2020 Research and Innovation Program (Project: ARIES-ULUND-LULAL-2019-01) and the Erlangen Graduate School in Advanced Optical Technologies (SAOT), which is funded by the state of Bavaria. We thank Ms. Sophie Sigl for supporting the image post-processing and data analysis.

References

[1] Fansler, T. D., Parrish, S. E., 2015, Measurement Science and Technology, 26(1), 012002.
[2] Berrocal, E., Conrad, C., Püls, J., Arnold, C. L., Wensing, M., Linne, M., Miranda, M., 2019, OSA Continuum, 2(3), pp. 983–993.
[3] Guénot, D., Svendsen, K., Björklund Svensson, J., Ekerfelt, H., Persson, A., Lundh, O., Berrocal, E., 2020, Optica, 7(2), pp. 131–134.
[4] Coghe, A., Cossali, G. E., 2012, Optics and Lasers in Engineering, 50(1), pp. 46–56.
[5] Linne, M., 2013, Progress in Energy and Combustion Science, 39(5), pp. 403–440.
[6] Rahm, M., Paciaroni, M., Wang, Z., Sedarsky, D., Linne, M., 2015, Optics express, 23(17), pp. 22444–22462.
[7] Berrocal, E., Kristensson, E., Hottenbach, P., Aldén, M., Grünefeld, G., 2012, Applied Physics B, 109(4), pp. 683–694.
[8] Breuninger, T., Greger, K., Stelzer, E. H. K., 2007, Optics letters, 32(13), pp. 1938–1940.
[9] Xu, C., Zipfel, W., Shear, J. B., Williams, R. M., Webb, W. W., 1996, Proceedings of the National Academy of Sciences of the United States of America, 93(20), pp. 10763–10768.
[10] Richardson, D. R., Roy, S., Gord, J. R., 2017, Optics letters, 42(4), pp. 875–878.
[11] Kulatilaka, W. D., Patterson, B. D., Frank, J. H., Settersten, T. B., 2008, Applied optics, 47(26), pp. 4672–4683.
[12] Frank, J. H., Chen, X., Patterson, B. D., Settersten, T. B., 2004, Applied optics, 43(12), pp. 2588–2597.
[13] Torelli, R., Som, S., Pei, Y., Zhang, Y., Traver, M., 2017, Fuel, 204(1), pp. 171–184.
[14] Zigan, L., Shi, J.-M., Krotow, I., Schmitz, I., Wensing, M., Leipertz, A., 2013, International Journal of Engine Research, 14(6), pp. 543–556.
[15] Lešnik, L., Kegl, B., Bombek, G., Hočevar, M., Biluš, I., 2018, Fuel, 222(1), pp. 550–560.
[16] Svendsen, K., González, I. G., Hansson, M., Svensson, J. B., Ekerfelt, H., Persson, A., Lundh, O., 2018, Optics express, 26(26), pp. 33930–33941.
[17] Zigan, L., Schmitz, I., Flügel, A., Wensing, M., Leipertz, A., 2011, Fuel, 90(1), pp. 348–363.
[18] Lemmon, E. W., Huber, M. L., McLinden, M. O., 2013, "REFPROP" 9.1 (Reference Fluid Thermodynamic and Transport Properties Database).
[19] Dean, J. A., Lange, N. A., 1999, "Lange's handbook of chemistry".
[20] Zigan, L.,Schmitz, I.,Wensing, M.,Leipertz, A." Sep. 6.-9., 2010, 23rd Annual Conference on Liquid Atomization and Spray Systems.